REVIEW

https://doi.org/10.1038/s41586-018-0491-6

Decoding the phase structure of QCD via particle production at high energy

Anton Andronic[1,2], Peter Braun-Munzinger[1,3,4]*, Krzysztof Redlich[1,5] & Johanna Stachel[3]

Recent studies based on lattice Monte Carlo simulations of quantum chromodynamics (QCD)—the theory of strong interactions—have demonstrated that at high temperature there is a phase change from confined hadronic matter to a deconfined quark–gluon plasma in which quarks and gluons can travel distances that greatly exceed the size of hadrons. Here we show that the phase structure of such strongly interacting matter can be decoded by analysing particle production in high-energy nuclear collisions within the framework of statistical hadronization, which accounts for the thermal distribution of particle species. Our results represent a phenomenological determination of the location of the phase boundary of strongly interacting matter, and imply quark–hadron duality at this boundary.

Atomic nuclei are bound by the strong force between their constituent 'nucleons': protons and neutrons. Although the density in the centre of a heavy nucleus is extremely large (about 10^{14} times the density of water), the mean distance between nucleons exceeds their diameter (the radius of the nucleon is about 0.88 fm = 0.88×10^{-15} m and the number density inside a nucleus is $n_0 = 0.16\ \mathrm{fm}^{-3}$). Thus, normal nuclear matter is a dilute many-body system. If such matter is compressed or heated in high-energy nuclear collisions (see, for example, refs [1–3]) to even higher densities or high temperatures (typically of the order of $k_\mathrm{B}T \approx m_\pi c^2$, where m_π is the mass of the lightest hadron (the pion), T is the temperature, k_B is Boltzmann's constant and c is the speed of light), then quarks, the building blocks of nucleons, are expected[4–7] to be no longer confined but able to move over distances much larger than the size of the nucleon. Such a 'deconfined' state of matter, named the quark–gluon plasma (QGP)[8], is likely to have existed in the early Universe within the first microseconds after the Big Bang[9]. One of the challenging questions in modern nuclear physics is to identify the structure and phases of such strongly interacting matter[10].

Evidence for the existence, in the laboratory, of the QGP has been obtained by studying collisions between heavy atomic nuclei (Au and Pb) at ultra-relativistic energies. The first relevant results came from experiments at the CERN (European Organization for Nuclear Research) Super Proton Synchrotron (SPS) accelerator[11]. Using the Relativistic Heavy Ion Collider (RHIC) at Brookhaven National Laboratory (BNL), experiments confirmed the existence of this new state of matter, providing further strong evidence for QGP formation and expansion dynamics in the hot fireball produced in high-energy nuclear collisions. Supporting evidence was also obtained from experiments at the BNL Alternating Gradient Synchrotron (AGS) through the discovery of collective dynamics at high energy[12]. For nuclear collisions, the centre-of-mass energies per nucleon pair, $\sqrt{s_\mathrm{NN}}$, covered by different accelerator facilities are: (1) the BNL AGS, $\sqrt{s_\mathrm{NN}} = 2.7$–$4.8$ GeV, (2) the CERN SPS, $\sqrt{s_\mathrm{NN}} = 6.2$–$17.3$ GeV, (3) the BNL RHIC, $\sqrt{s_\mathrm{NN}} = 7.0$–$200$ GeV and (4) the CERN Large Hadron Collider (LHC), $\sqrt{s_\mathrm{NN}} = 2.76$–$5.02$ TeV.

The results from RHIC showed that the QGP behaves more like a nearly ideal, strongly interacting fluid than a weakly interacting gas of quarks and gluons[1,3,13–16]. These results were confirmed and extended into hitherto unexplored regions of phase space (in particular, high transverse momenta) by experiments at the CERN Large Hadron Collider (LHC)[17–19]. At LHC energies, the fireball formed in Pb–Pb collisions is so hot and dense that quarks or gluons (partons) produced initially with energies of up to a few hundred gigaelectronvolts lose a substantial fraction of their energy while traversing it.

The characterization of the QGP in terms of its equation of state (which expresses pressure as a function of energy density) and of its transport properties (such as its viscosity or diffusion coefficients) as well as delineating the phases of strongly interacting matter[20] is a major ongoing research effort[2,3,18,21,22]. However, it has turned out that direct connections between the underlying theory of strong interactions in the standard model of particle physics, QCD[23] and the experimental data are not readily to be established. This is because the constituents of the QGP—the coloured quarks and gluons—are not observable as free particles, a fundamental property of QCD called 'confinement'. What is observable are colourless bound states of these partons, resulting in mesons and baryons; these bound states are generally referred to as hadrons. Furthermore, the equations of QCD can be solved analytically only in the high-energy and short-distance limit where perturbative techniques can be used owing to the asymptotic freedom property of QCD[24,25]. This is unfortunately not possible for the QGP, where typical distance scales exceed the size of the largest atomic nuclei and the typical momentum scale is low. The only technique known at present is lattice QCD (LQCD)[26], whereby the QCD equations are solved numerically by discretizing the QCD Lagrangian on a four-dimensional space-time lattice and evaluating them statistically via Monte Carlo methods.

In the following sections we discuss how the phase structure of strongly interacting matter described by LQCD can be decoded by analysing particle production in high-energy nuclear collisions. This is achieved by using the observed thermalization pattern of particle abundances within the framework of statistical hadronization at various collision energies.

Connecting hadronic states and QCD constituents

From LQCD calculations, a deconfinement transition from matter composed of hadronic constituents (that is, hadronic matter) to a QGP has indeed been predicted (see ref. [26] for an early review) at an energy density of about 1 GeV fm^{-3}. Besides deconfinement, there is also a

[1]Research Division and EMMI, GSI Helmholtzzentrum für Schwerionenforschung, Darmstadt, Germany. [2]Institut für Kernphysik, Universität Münster, Münster, Germany. [3]Physikalisches Institut, Universität Heidelberg, Heidelberg, Germany. [4]Institute of Particle Physics and Key Laboratory of Quark and Lepton Physics (MOE), Central China Normal University, Wuhan, China. [5]University of Wrocław, Institute of Theoretical Physics, Wrocław, Poland. *e-mail: p.braun-munzinger@gsi.de

chiral symmetry restoration transition expected in high-energy-density matter[27,28].

Owing to the very small masses of the up and down quarks, the equations of QCD exhibit symmetries, called chiral symmetries, that allow separate transformations among the right-handed quarks (with spin oriented in the direction of momentum) and left-handed quarks. Such symmetries, however, are not manifest in the observed strongly interacting particles; these particles do not come in opposite-parity pairs. Thus, chiral symmetry must be spontaneously broken at finite energy density. Consequently, QCD predicts the existence of a chiral transition between a phase in which chiral symmetry is broken, at low temperature or density, and a chirally symmetric phase at high temperature or density. The connection between deconfinement and chiral transition is theoretically not fully understood.

It has been demonstrated[29], again using the methods of LQCD, that at zero baryo-chemical potential μ_b the deconfinement transition is linked to the restoration of chiral symmetry and that it is of crossover type with a continuous, smooth but rapid increase of thermodynamic quantities in a narrow region around the pseudo-critical temperature T_c. Henceforth using units such that $\hbar = 1$, $k_B = 1$ and $c = 1$, the value of T_c at vanishing μ_b is currently calculated in LQCD to be 154 ± 9 MeV[30] and 156 ± 9 MeV[31,32] with different fermion actions, in excellent agreement (uncertainties quoted here and elsewhere are the standard error of the mean). Recent LQCD results also quantify the small decrease of T_c with increasing μ_b as long as $\mu_b < 3T_c$. Within this parameter range the transition is still of crossover type. A fundamental question is the possible existence of a critical endpoint, where a genuine second-order chiral phase transition is expected. This has been addressed both experimentally (see a review in ref. [33]) and theoretically (see a review in ref. [34]) but remains one of the outstanding questions related to our understanding of the phase structure of hot and dense QCD matter.

These results do not shed light on the mechanism of the transition from deconfinement to confinement. In fact, the crossover nature of the chiral transition raises the question whether hadron production from a deconfined medium might also happen over a wide range of temperatures and how confinement can be implemented in a smooth transition without leading to free quarks. A related question is whether colourless bound states (hadrons) might survive in a deconfined medium. The present work attempts to shed light on some of these questions by connecting LQCD phenomenology and the impressive body of results on hadron production in central collisions between two heavy atomic nuclei at high energy. Central collisions are nearly head-on collisions; centrality is calculated in experiments matching measured particle multiplicity or energy to the geometry of the collision (see details in ref. [17]).

The QCD Lagrange density is formulated entirely in terms of the basic constituents of QCD, the quarks and gluons. The masses of hadrons as colourless bound states of quarks and gluons are well calculated within LQCD, showing remarkable agreement with experiment[35]. This confirms that chiral symmetry is broken in the QCD vacuum, as reflected in the mass differences between parity partners as well as the existence of anomalously light pions as approximate Goldstone bosons associated with spontaneous symmetry breaking.

One of the consequences of confinement in QCD is that physical observables require a representation in terms of hadronic states. Indeed, as has been noted recently in the context of QCD thermodynamics (see ref. [36] and references therein) the corresponding partition function Z can be very well approximated within the framework of the hadron resonance gas, as long as the temperature stays below T_c. To make this more transparent, we first note that all thermodynamic variables, such as pressure P and entropy density can be expressed in terms of derivatives of logarithms of Z. For P, for example, we obtain for a system with volume V and temperature T:

$$\frac{P}{T^4} = \frac{1}{T^3}\frac{\partial \ln[Z(V,T,\boldsymbol{\mu})]}{\partial V} \tag{1}$$

The results of refs [37–42] imply that, as long as $T \leq T_c$,

$$\ln[Z(T,V,\boldsymbol{\mu})] \approx \sum_{i\in\text{mesons}} \ln[Z_{m_i}(T,V,\mu_Q,\mu_s)] + \sum_{i\in\text{baryons}} \ln[Z_{m_i}(T,V,\mu_b,\mu_Q,\mu_s)] \tag{2}$$

where the partition function of the hadron resonance gas model is expressed in mesonic and baryonic components, where m_i is the mass of a given hadron. The chemical potential $\boldsymbol{\mu}$ then reflects the baryonic, electric charge and strangeness components $\boldsymbol{\mu} = (\mu_b, \mu_Q, \mu_s)$.

To make this connection quantitative, detailed investigations have recently been made into the contribution of mesons and baryons to the total pressure of the matter. In particular, in refs [36,38] and references therein, the equation of state and different fluctuation observables are evaluated in the hadronic sector via the hadron resonance gas and compared to predictions from LQCD. Very good agreement is obtained for temperatures up to very close to T_c, lending further support to the hadron–parton duality described by equation (2).

The partition function of the hadron resonance gas in equation (2) is evaluated as a mixture of ideal gases of all stable hadrons and resonances. In the spirit of the S-matrix formalism[39], which provides a consistent theoretical framework to implement interactions in a dilute many-body system in equilibrium, the presence of resonances corresponds to attractive interactions among hadrons. This is generally a good approximation, because for the temperatures considered here ($T < 165$ MeV) the total particle density is low, $n < 0.5$ fm^{-3}.

Sometimes, additional repulsive interactions are modelled with an 'excluded volume' prescription (see ref. [37] and references therein), which is inherently a low-density approach. For weak repulsion, implying excluded volume radii of $r_0 < 0.3$ fm, the effect of the correction is mainly to decrease particle densities, whereas the important thermal parameters T and μ_b are little affected. Strong repulsion cannot be modelled that way: much larger r_0 values lead to, among others, unphysical (superluminous) equations of state, in contradistinction to results from LQCD. In the following we use $r_0 = 0.3$ fm for both mesons and baryons. All results on thermal parameters described below are unchanged from what is obtained in the non-interacting limit except for the overall particle density, which is reduced by up to 25%.

Over the course of the past 20 years it has become apparent[40–45] that the yields of all hadrons produced in central collisions can be very well described by computing particle densities from the hadronic partition function described by equation (2). To obtain particle yields at a particular temperature T_{cf} and μ_b one multiplies the thermal densities obtained in this way with the fireball volume V. In practice, T_{cf}, μ_b and V, the parameters at 'chemical freeze-out' from which point on all hadron yields are frozen, are determined from a fit to the experimental data. We note that V is actually the volume that corresponds to a slice of one unit of rapidity y, centred at mid-rapidity. Experimentally, the rapidity density $\mathrm{d}N/\mathrm{d}y$ of a hadron is obtained by integrating its momentum-space distribution over the momentum component transverse to the beam direction. In general we take these yields N at mid-rapidity ($y = 0$), where the centre of mass of the colliding system is at rest.

As will be discussed below, this 'statistical hadronization approach' provides, via equations (1) and (2), a link between data on hadron production in ultra-relativistic nuclear collisions and the QCD partition function. This link may shed light on the QCD phase diagram. The possibility of such a connection was surmised early on[6,46] and various aspects of it have been discussed more recently[44,47–53].

The full power of this link, however, becomes apparent only with the recent precision data from the LHC. Below, we discuss the accuracy that can be achieved in the description of hadron production using the parton–hadron duality concept described by equation (2). We first focus on hadrons that contain only light quarks with flavours up, down and strange (u, d and s) and place emphasis on LHC data. Those show matter and antimatter production in equal amounts, thus indicating that μ_b is very close to zero. It is in this energy region that the LQCD

approach can be applied essentially without approximations using current computer technology. We then explore the lower-energy region (500 GeV $> \sqrt{s_{NN}} >$ 15 GeV) and show that consistent information on the QCD phase diagram for $0 < \mu_b < 300$ MeV can be achieved by quantitatively comparing LQCD predictions for finite μ_b with results from statistical hadronization analysis of hadron production data. In section 'Statistical hadronization of heavy quarks' we discuss how the statistical hadronization approach can be extended to include heavy (charm *c* and bottom *b*) quarks. We further discuss how the recent LHC data can provide information on the hadronization of these heavy quarks during the expansion and cooling of the QGP formed in such high-energy central nuclear collisions.

Statistical hadronization of light quarks

The description of particle production in nucleus–nucleus collisions in the framework of the statistical hadronization approach is particularly transparent at the LHC energy where the chemical freeze-out is quantified, essentially, by the temperature T_{cf} and the volume V of the fireball produced.

The parameters of the statistical hadronization approach are obtained with considerable precision by comparison with the yields of particles measured by the ALICE Collaboration[54–60]. To match the measurement, the calculations include all contributions from the strong and electromagnetic decays of high-mass resonances. For $\pi^{\pm}$, $K^{\pm}$ and K^0 mesons, the contributions from heavy-flavour hadron decays are also included. The measurement uncertainty σ is accounted for as the quadratic sum of statistical and systematic uncertainties; see below.

For the most central Pb–Pb collisions, the best description of the ALICE data on yields of particles in one unit of rapidity at mid-rapidity is obtained with $T_{cf} = 156.5 \pm 1.5$ MeV, $\mu_b = 0.7 \pm 3.8$ MeV and $V = 5{,}280 \pm 410$ fm^3. This result is an update of the previous analysis from ref. [45] using an extended and final dataset. The standard deviations quoted here are exclusively due to experimental uncertainties and do not reflect the systematic uncertainties connected with the model implementation, as discussed below.

Remarkably, the values of the chemical freeze-out temperature $T_{cf} = 156.5 \pm 1.5$ MeV and the pseudo-critical temperature $T_c = 154 \pm 9$ MeV obtained in LQCD agree within errors. This implies that chemical freeze-out takes place close to hadronization of the QGP, lending support also to the hadron–parton duality described by equation (2).

A comparison of the statistical hadronization results obtained with the thermal parameters discussed above and the ALICE data for particle yields is shown in Fig. 1. Impressive overall agreement is obtained between the measured particle yields and the statistical hadronization analysis. The agreement spans nine orders of magnitude in abundance values, encompasses strange and non-strange mesons, baryons including strange and multiply strange hyperons as well as light nuclei and hypernuclei and their antiparticles. A very small value for the baryo-chemical potential $\mu_b = 0.7 \pm 3.8$ MeV, consistent with zero, is obtained, as is expected from the observation of the equal production of matter and antimatter at the LHC[61].

The largest difference between the data and calculations is observed for proton and antiproton yields, where a deviation of 2.7σ is obtained. This difference is connected with an unexpected and puzzling centrality dependence of the ratio $(p + \overline{p})/(\pi^+ + \pi^-)$ (see figure 9 of ref. [54]). As discussed below, the other ratios (hadrons/pions) increase towards more central collisions until a plateau (the grand-canonical limit) is reached. The peculiar behaviour of the $(p + \overline{p})/(\pi^+ + \pi^-)$ ratio at LHC energy is currently not understood. Arguments that this might be connected to annihilation of baryons in the hadronic phase after chemical freeze-out[62] are not supported by the results of recent measurements of the relative yields of strange baryons to pions[63].

A further consequence of the vanishing baryo-chemical potential is that the strangeness chemical potential μ_s also vanishes. This implies that the strangeness quantum number no longer affects the particle production. In the fireball the yield of strange mesons and (multi-) strange baryons is exclusively determined by their mass m and spin degeneracy $(2J + 1)$ in addition to the temperature T.

The thermal origin of all particles including light nuclei and antinuclei is particularly transparent when inspecting how their yields change with particle mass. This is shown in Fig. 2, where the measured yields, normalized to the spin degeneracy, are plotted as a function of the mass m. This demonstrates explicitly that the normalized yields depend exclusively on m and T. For heavy particles ($m \gg T$) without resonance decay contributions their normalized yield simply scales with mass as $m^{3/2}\exp(-m/T)$, illustrated by the nearly linear dependence observed in the logarithmic representation of Fig. 2. We note that, for the subset of light nuclei, the statistical hadronization predictions are not affected by resonance decays. For these nuclei, a small variation in temperature leads to a large variation of the yield, resulting in a relatively precise determination of the freeze-out temperature $T_{nuclei} = 159 \pm 5$ MeV, consistent with the value of T_{cf} extracted above.

The incomplete knowledge of the structure and decay probabilities of heavy mesonic and baryonic resonances discussed above leads to systematic uncertainties in the statistical hadronization approach. We note from Fig. 2 that the yields of the measured lightest mesons and baryons (π, K, p and Λ) are substantially increased relative to their primordial thermal production by such decay contributions. For pions, for example, the resonance decay contribution amounts to 70%. For resonance masses larger than 1.5 GeV the individual states start to overlap strongly[23]. Consequently, neither their number density nor their decay probabilities can be well determined. Indeed, recent LQCD results indicate that there are missing resonances compared to what is listed in ref. [23]. The resulting theoretical uncertainties are difficult to estimate but are expected to be small because T_{cf} is very small compared to the mass of the missing resonances. A conservative estimate is that the resulting systematic uncertainty in T_{cf} is at most 3%. This is consistent with the determination of T_{cf} using only particles whose yields are not influenced by resonance decays (see above). Until now, none of these systematic uncertainties are taken into account in the statistical hadronization analysis described here.

The rapidity densities of light (anti-)nuclei and hypernuclei have been predicted[64] on the basis of the systematics of hadron production at lower energies. It is nevertheless remarkable that such loosely bound objects (the deuteron binding energy is 2.2 MeV, much less than $T_{nuclei} \approx 159$ MeV or $T_{cf} \approx T_c \approx 155$ MeV) are produced with temperatures very close to that of the phase boundary at LHC energy, implying that any further evolution of the fireball has to be close to isentropic. For the hypertriton ${}^3_{\Lambda}H$ and antihypertriton ${}^3_{\Lambda}\overline{H}$, the situation is even more dramatic: this object consists of a bound state of (p, n, Λ), with an energy of only 130 ± 30 keV needed to remove the Λ particle from the bound state. This implies that the Λ particle is very weakly bound to a deuteron, resulting in root-mean-square size for this bound state of close to 10 fm, about the same size as that of the fireball formed in the Pb–Pb collision.

The detailed production mechanism for loosely bound states remains an open question. One, admittedly speculative, possibility is that such objects, at QGP hadronization, are produced as compact, colourless droplets of quark matter with quantum numbers of the final-state hadrons. The concept of possible excitations of nuclear matter into colourless quark droplets has already been considered[65]. In the context of our work, these states should have a lifetime of 5 fm or longer, with excitation energies of 40 MeV or less, for evolution into the final-state hadrons that are measured in the detector. Since by construction they are initially compact, they would also survive a possible short-lived hadronic phase after hadronization. This would be a natural explanation for the striking observation of the thermal pattern for these nuclear bound states emerging from Figs. 1, 2. We note that the observed thermal nature of the production yields of the nuclear bound states is very difficult to reconcile with the assumption that these states are formed by coalescence of baryons, where the yield is proportional to a coalescence factor introduced as the square of the nuclear wavefunction, which varies widely among the various nuclei[66,67]. For a recent discussion of the application of coalescence models to production of loosely bound states, see ref. [68].

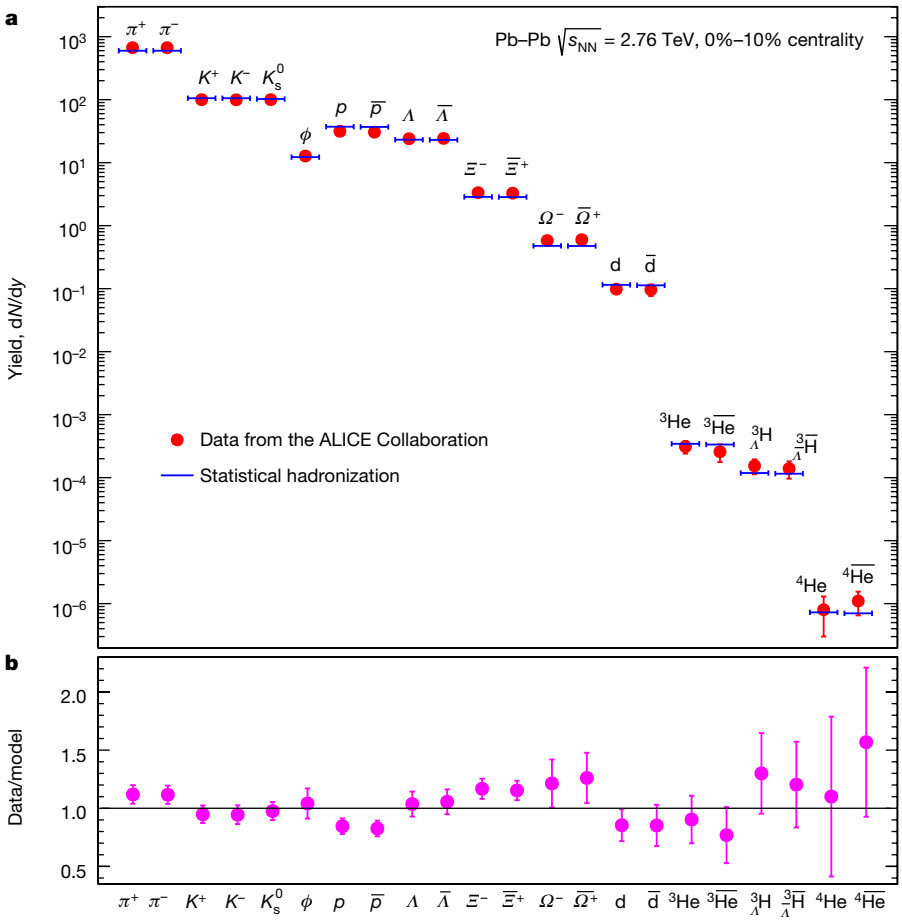

Fig. 1 | Hadron abundances and predictions of the statistical hadronization model. a, dN/dy values for different hadrons and nuclei, measured at mid-rapidity (red circles), including the hypertriton ${}^{3}_{\Lambda}H$, are compared with the statistical hadronization analysis (blue bars). The data are from the ALICE Collaboration for central Pb–Pb collisions at the LHC[53–59]. **b**, The ratio of the data to statistical hadronization predictions (model), with errors bars determined only from the data as the quadratic sum of statistical and systematic uncertainties.

It could be argued that composite particles such as light nuclei and hypernuclei should not be included in the hadronic partition function described in equation (2). However, all nuclei, including light, loosely bound states, should result from the interaction of the fundamental QCD constituents. This is confirmed by recent LQCD calculations[69].

The thermal nature of particle production in ultra-relativistic nuclear collisions has been experimentally verified not only at LHC energy, but also at the lower energies of the RHIC, SPS and AGS accelerators. The essential difference is that, at these lower energies, the matter–antimatter symmetry observed at the LHC is lifted, implying non-vanishing values of the chemical potentials. Furthermore, in central collisions at energies below $\sqrt{s_{NN}} \approx 6$ GeV the cross-section for the production of strange hadrons decreases rapidly, with the result that the average strange hadron yields per collision can be far below unity. In this situation, one needs to implement exact strangeness conservation in the statistical sum in equation (2) and apply the canonical ensemble for the conservation laws[70,71]. Similar considerations apply for the description of particle yields in peripheral nuclear and elementary collisions. An interesting consequence of exact strangeness conservation is a suppression of strange particle yields when going from central to peripheral nucleus–nucleus collisions or from high multiplicity to low multiplicity events in proton–proton or proton–nucleus collisions. In all cases the suppression is further enhanced with increasing strangeness content of the hadron. Sometimes, additional fugacity parameters g_f are introduced to account for possible non-equilibrium effects of strange- and heavy-flavour hadrons[44,72]. These parameters modify the thermal yields of particles by factors $g_f^{n_f}$, where the power n_f denotes the number of strange or heavy quarks and antiquarks in the hadron.

Experimental consequences of canonical thermodynamics and strangeness conservation laws have been first seen at SPS energy[73]. All the above predictions are qualitatively confirmed by the striking results from high-multiplicity proton–proton and p–Pb collisions from the ALICE Collaboration at LHC energy[63]. The data also explicitly exhibit the plateau in strangeness production for Pb–Pb collisions, which is to be expected when the grand-canonical region is reached, further buttressing the thermal analysis discussed above.

An intriguing observation, first made in ref. [74], is that the overall features of hadron production in e^+e^- annihilations resemble that expected from a thermal ensemble with temperature $T \approx 160$ MeV, once exact quantum number conservation is taken into account. In these collisions, quark–antiquark pairs are produced with production yields that are not thermal but are well explained by the electro-weak standard model; see, for example, table 2 in ref. [75]. Hadrons from these quark pairs (and sometimes gluons) appear as jets in the data. The underlying hadronization process can be well described using statistical hadronization model ideas[75,76]. These studies reveal further that strangeness production deviates noticeably from a pure thermal production model and that the quantitative description of the measured yields is rather poor. Nevertheless, recognizable thermal features in e^+e^- collisions, where equilibration should be absent, may be a consequence of the generic nature of hadronization in strong interactions.

From a statistical hadronization analysis of all measured hadron yields at various beam energies the detailed energy dependence of the thermal parameters T_{cf} and μ_b has been determined[41,42,51,77–81]. While μ_b decreases smoothly with increasing energy, the dependence of T_{cf} on energy exhibits a striking feature that is illustrated in Fig. 3: T_{cf} increases with increasing energy (decreasing μ_b) from about 50 MeV

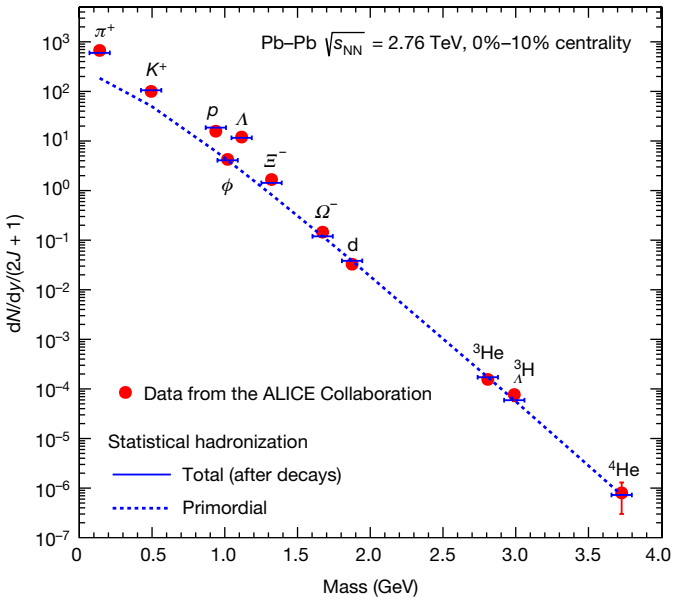

Fig. 2 | Mass dependence of hadron yields compared with predictions of the statistical hadronization model. Only particles (no antiparticles) are included and yields are divided by the spin degeneracy factor $(2J+1)$. Data are from the ALICE Collaboration for central Pb–Pb collisions at the LHC. For the statistical hadronization approach, the 'total' yields (blue bars) include all contributions from high-mass resonances (for the Λ hyperon, the contribution from the electromagnetic decay $\Sigma^0 \rightarrow \Lambda\gamma$, which cannot be resolved experimentally, is also included); the primordial yields before strong and electromagnetic decays are plotted as the dotted line. For more details, see the main text.

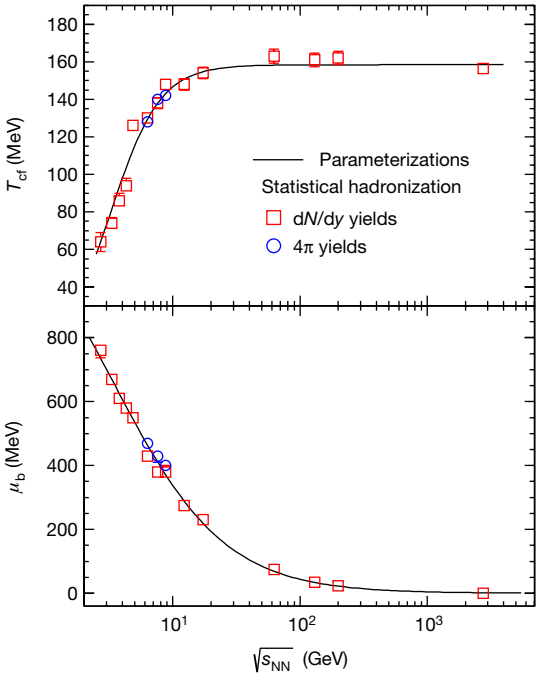

Fig. 3 | Energy dependence of chemical freeze-out parameters T_{cf} and μ_b. The results are obtained from the statistical hadronization analysis of hadron yields (at mid-rapidity, dN/dy, and in full phase space, 4π) for central collisions at different energies. The parameterizations shown are: $T_{cf} = T_{cf}^{lim}/\{1+\exp[2.60-\ln(\sqrt{s_{NN}})/0.45]\}$ and $\mu_b = a/(1+0.288\sqrt{s_{NN}})$, with $\sqrt{s_{NN}}$ in gigaelectronvolts, T_{cf}^{lim} =158.4 MeV and a = 1,307.5 MeV. The uncertainty of the limiting temperature T_{cf}^{lim}, determined from the fit of the five points that represent the highest energies, is 1.4 MeV.

to about 160 MeV, where it exhibits a saturation for $\sqrt{s_{NN}} > 20$ GeV. The slight increase of this value compared to T_{cf} = 156.5 MeV obtained at LHC energy is due to the inclusion of some data at RHIC energies, but the details of this small difference are currently not fully understood.

The saturation of T_{cf} observed in Fig. 3 lends support to the earlier proposal[48,50,82] that, at least at high energies, the chemical freeze-out temperature is very close to the QCD hadronization temperature[51], implying a direct connection between data from relativistic nuclear collisions and the QCD phase boundary. This is in accord with the earlier prediction, more than 50 years ago[83,84], that hadronic matter cannot be heated beyond this limit. Whether there exists, at lower energies, a critical endpoint[85] in the QCD phase diagram is currently at the focus of intense theoretical[19] and experimental effort[77].

To illustrate how well the thermal description of particle production in central nuclear collisions works we show, in Fig. 4, the energy dependence (excitation function) of the relative abundance of several hadron species along with the prediction using the statistical hadronization approach and the smooth evolution of the parameters (see above). Because of the interplay between the energy dependence of T_{cf} and μ_b there are characteristic features in these excitation functions. In particular, maxima appear at slightly different center-of-mass energies in the K^+/π^+ and Λ/π^+ ratios, whereas the corresponding antiparticle ratios exhibit a smooth behaviour[86].

In the statistical approach in equation (2) and in the Boltzmann approximation, the density $n(\mu_b, T)$ of hadrons carrying baryon number B scales with the chemical potential as $n(\mu_b,T) \propto \exp(B\mu_b/T)$. Consequently, the ratios p/π^+ and d/p, where d refers to a deuteron, scale as $\exp(\mu_b/T)$, whereas the corresponding antiparticle ratios scale as $\exp(-\mu_b/T)$. From Fig. 3, it is apparent that μ_b/T_{cf} decreases with collision energy, accounting for the basic features of particle ratios in the upper panel of Fig. 4. On the other hand, strangeness conservation unambiguously connects, for every T value, the strangeness potential and the baryo-chemical potential, $\mu_s = \mu_s(\mu_b)$. As a consequence, the yields of K^+ and K^- increase and, respectively, decrease with μ_b/T. At higher energies, where T and hence pion densities saturate, the Λ/π^+ and K^+/π^+ ratios are decreasing with energy (see lower panel of Fig. 3).

We further note that, for energies beyond that of the LHC, the thermal parameter T_{cf} is determined by the QCD pseudo-critical temperature and the value of μ_b vanishes. Combined with the energy dependence of overall particle production[87] in central Pb–Pb collisions, this implies that the statistical hadronization model prediction of particle yields at any energy, including those at the possible Future Circular Collider (FCC)[88] or in ultrahigh-energy cosmic ray collisions[89], can be made with an estimated precision of better than 15%.

Since the statistical hadronization analysis at each measured energy yields a pair of (T_{cf}, μ_b) values, these points can be used to construct a T versus μ_b diagram, describing phenomenological constraints on the phase boundary between hadronic matter and the QGP; see Fig. 5. We note that the points at low temperature seem to converge towards the value for ground-state nuclear matter (μ_b = 931 MeV). As argued previously[52], this limit is not necessarily connected to a phase transition. Although the situation at low temperatures and collision energies is complex and at present cannot be investigated with first-principles calculations, the high-temperature, high-collision energy limit allows a quantitative interpretation in terms of fundamental QCD predictions.

The connection between LQCD predictions and experimental chemical freeze-out points is made quantitative in Fig. 5. We use here recent results for the QCD phase boundary from the two leading LQCD groups[30,90], represented by the band in Fig. 5. As can be seen, the LQCD values follow the measured μ_b dependence of the chemical freeze-out temperature very closely, demonstrating that with relativistic nuclear collisions one can directly probe the QCD phase boundary between hadronic matter and the QGP. The above results imply that the pseudo-critical temperature of the QCD phase boundary at $\mu_b = 0$ as well as its μ_b dependence up to μ_b = 300 MeV have been determined experimentally. There is indirect but strong evidence from measurements of the initial energy density as well as from hydrodynamical analysis of transverse momentum spectra and from the analysis of jet quenching

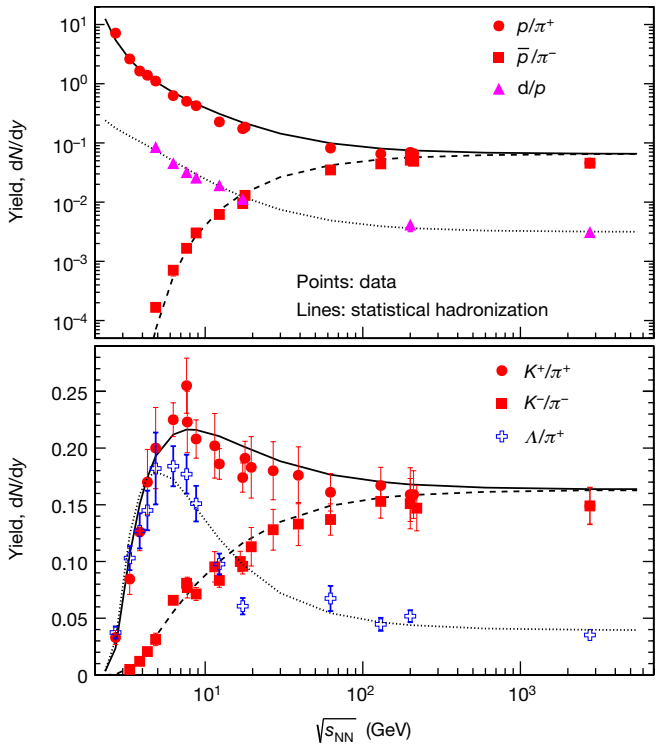

Fig. 4 | Collision-energy dependence of the relative abundance of several hadron species. The data for central collisions (symbols) are compiled from refs [77,131], and are compared to statistical hadronization calculations for the smooth parameterizations of T_{cf} and μ_b as functions of energy shown in Fig. 3.

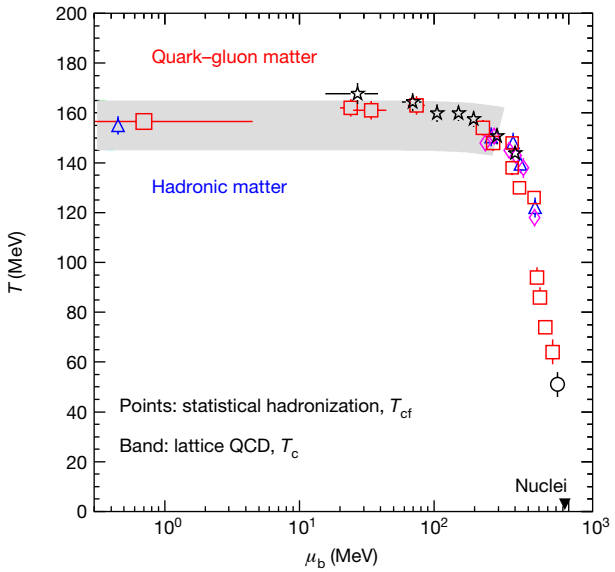

Fig. 5 | Phenomenological phase diagram of strongly interacting matter. The diagram is constructed from chemical freeze-out points that result from statistical hadronization analysis of hadron yields for central collisions at different energies. The freeze-out points, with error bars showing the standard error of the mean, extracted from experimental datasets in our own analysis (red squares) and other similar analyses[77,78,132,133] (other symbols), are compared to predictions from LQCD[30,90] (grey band). The inverted triangle marks the value for ground-state nuclear matter (atomic nuclei). The colouring of the labels 'quark–gluon matter' and 'hadronic matter' indicates the temperature of the matter.

data that the initial temperatures of the fireball formed in the collision are substantially higher than the values at the phase boundary, reaching 300–600 MeV at RHIC and LHC energies[91,92].

The present approach can be extended beyond hadron yields to higher moments of event-by-event particle distributions. Although precision predictions from LQCD exist for higher moments and susceptibilities, especially at LHC energies where μ_b is close to zero (see, for example, refs [36,38]), there are formidable difficulties in experimentally determining such higher moments with accuracy. Pioneering experiments were performed at the RHIC accelerator with intriguing but not yet fully conclusive results; for a recent review see ref. [33]. Analyses of higher moments are, therefore, not considered here. Recently, however, the variances (second moments) of strangeness and net-baryon-number fluctuations were reconstructed[93] from hadron yields measured in Pb–Pb collisions at mid-rapidity by the CERN ALICE Collaboration. The second moments determined in this way are in impressive agreement with LQCD predictions obtained at the chiral crossover pseudo-critical temperature $T_c \approx 154$ MeV. Furthermore, an interesting strategy was proposed to directly compare experimental data on moments of net-charge fluctuations with LQCD results to identify freeze-out parameters in heavy ion collisions[94]. Within still large systematic uncertainties the extracted freeze-out parameters based on second-order cumulants are consistent with statistical hadronization[95,96]. Although no formal proof of the above discussed quark–hadron duality near the chiral crossover temperature exists, the empirical evidence has recently clearly been strengthened.

Statistical hadronization of heavy quarks

An interesting question is whether the production of hadrons with heavy quarks can be described with similar statistical hadronization concepts as developed and used in the previous section for light quarks. We note first that the masses of charm and beauty quarks, $m_c = 1.28$ GeV and $m_b = 4.18$ GeV, are much larger than the characteristic scale of QCD, $\Lambda_{QCD} = 332$ MeV for three quark flavours, in the modified minimal subtraction scheme[23]. Both masses are also sufficiently larger than the pseudo-critical temperature T_c introduced above, such that thermal production of charm and, in particular, beauty quarks is strongly Boltzmann-suppressed. This is also borne out by quantitative calculations[97–99]. On the other hand we expect, in particular at LHC energies, copious production of heavy quarks in relativistic nuclear collisions through hard scattering processes which, in view of the large quark masses, can be well described using QCD perturbation theory[100]. Consequently, the charm and beauty content of the fireball formed in the nucleus–nucleus collision is determined by the initial hard scattering. Furthermore, the annihilation of charm and beauty quarks is very small, implying that their numbers are tightly preserved during the fireball evolution[101].

The charm quarks produced will, therefore, not resemble a chemical equilibrium population for temperature T. However, what is needed for the thermal description proposed below is that the heavy quarks produced in the collision reach a sufficient degree of thermal equilibrium through scattering with the partons of the hot medium. Indeed, the energy loss suffered by energetic heavy quarks in the QGP is indicative of their 'strong coupling' with the medium, dominated by light quarks and gluons. The measurements at the LHC[102,103] and RHIC[104] of the energy loss and hydrodynamic flow of D mesons demonstrate this quantitatively.

Of the various suggested probes of deconfinement, charmonium (the bound state of the charm and anticharm quarks, $c\bar{c}$) is particularly interesting. The J/ψ meson (the ground state of charmonium) is the first hadron for which a clear mechanism of suppression (melting) in the QGP was proposed early on, based on the colour analogue of Debye screening[105]. This concept for charmonium suppression was tested experimentally at the SPS accelerator but led, with the turn-on of the RHIC facility, to a number of puzzling results. In particular, the observed rapidity and energy dependence of the suppression ran counter to the theoretical predictions[106].

However, before publication of the first RHIC data, a quarkonium production mechanism based on statistical hadronization, was proposed[72] that contained a natural explanation for the later observations at RHIC and LHC energy. The basic concept underlying this

statistical hadronization approach[72] is that charm quarks are produced in initial hard collisions, subsequently thermalize in the QGP and are 'distributed' into hadrons at the phase boundary, that is, at chemical freeze-out, with thermal weights as discussed above for the light quarks[72,101,107,108]. An alternative mechanism for the (re)combination of charm and anticharm quarks into charmonium in a QGP[109] has been proposed, based on kinetic theory. For further developments see refs [110–113].

In the statistical hadronization approach, the absence of chemical equilibrium for heavy quarks is accounted for by introducing a fugacity g_c. The parameter g_c is obtained from the balance equation[72], which accounts for the distribution of all initially produced heavy quarks into hadrons at the phase boundary, with a thermal weight constrained by exact charm conservation. Using this approach, the knowledge of the heavy-quark production cross-section along with the thermal parameters obtained from the analysis of the yields of hadrons composed of light quarks (see section 'Statistical hadronization of light quarks') is sufficient to determine the yield of hadrons containing heavy quarks in ultra-relativistic nuclear collisions.

As a consequence, a very useful observable with which to verify the thermal origin of heavy-flavour hadrons produced in a nuclear collision is the abundance ratio of different resonance states such as $\psi(2S)/(J/\psi)$ in the charm-sector or $\Upsilon(2S)/\Upsilon(1S)$ in the bottom-sector (where bottomonium Υ is the bound state of the bottom and antibottom quarks, $b\bar{b}$). Indeed, the first measurement of the $\psi(2S)/(J/\psi)$ abundance ratio at the SPS energy[114] demonstrated that there are clearly different production mechanisms for charmonia in elementary and nuclear collisions. This is demonstrated in Fig. 6. Whereas in elementary collisions this ratio is roughly 0.15 and hardly varies with energy, the value observed in central Pb–Pb collisions is more than a factor of four smaller and is remarkably consistent with the assumption that these charmonia are produced at the phase boundary, as are all other hadrons.

The chemical freeze-out temperature barely varies with energy beyond $\sqrt{s_{NN}} = 10$ GeV. Because the charm production cross-section drops out in the $\psi(2S)/(J/\psi)$ ratio, the prediction of the statistical hadronization model for central Pb–Pb collisions at LHC energy is $\psi(2S)/(J/\psi) = 0.035$, with the precision indicated in Fig. 6. Recently, the ALICE Collaboration released the first (transverse momentum integrated) data on the above ratio; the preliminary result is, within the still considerable experimental uncertainties, consistent with the statistical hadronization prediction, lending further support for the thermalization of charm quarks in the hot fireball and the production of charmed hadrons at the phase boundary.

It is also important to assess to what degree the charmonia produced participate in the hydrodynamic expansion of the fireball. This can be done by measuring the second Fourier coefficient of the angular distribution of J/ψ mesons projected onto a plane perpendicular to the beam direction, the so-called elliptic flow. The first measurement of J/ψ elliptic flow at the LHC[115] pointed towards rather large values of the elliptic flow coefficients. The recent measurement at $\sqrt{s_{NN}} = 5.02$ TeV from the ALICE Collaboration[116] establishes the detailed flow pattern as a function of transverse momentum. The large elliptic flow observed for J/ψ mesons is similar to that observed for open charm mesons[117] (mesons that contain one charm quark or antiquark) and is surprisingly close to the flow coefficients for light hadrons. This provides strong support for charm quark kinetic thermalization, in agreement with the statistical hadronization assumption, and implies that charm quarks couple to the medium in a similar way as do light-flavour quarks. Within the current statistical accuracy the J/ψ data at RHIC are compatible with a null flow signal[118]. An elliptic anisotropy signal was measured for J/ψ mesons at SPS energy[119] and was interpreted as a path-length dependence of the screening.

The response of charmonia produced in ultra-relativistic nuclear collisions to the medium of the fireball is characterized by the nuclear modification factor R_{AA}. This factor is constructed as the ratio between the rapidity densities for J/ψ mesons produced in nucleus–nucleus (AA) collisions and proton–proton collisions, scaled by the number

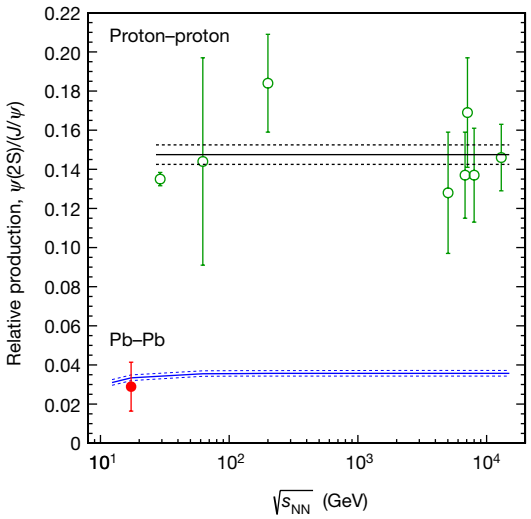

Fig. 6 | Relative production of $\psi(2S)$ and J/ψ mesons as a function of collision energy. The data points for proton–proton collisions are from experiments at SPS, the Hadron-Electron Ring Accelerator (HERA), RHIC and the LHC[134–139]. The point for central Pb–Pb collisions at the SPS energy is from the NA50 experiment[114]. The average value of the proton–proton measurements is represented by the black horizontal line with dashed uncertainties. The blue band denotes statistical model calculations for the temperature parameterization from heavy-ion fits; see Fig. 3. The errors on the data are the quadratic sum of statistical and systematic uncertainties.

of nucleon–nucleon collisions in a given centrality bin. Clearly, if all charmonia in the final state originate from hard scattering processes in the initial state, then $R_{AA} = 1$.

In the original colour-screening model[105], R_{AA} was expected to be significantly reduced from unity and to decrease with collision centrality and energy, owing to the increasing energy density of the medium. The early experimental situation until 2009, that is, before LHC turn-on, is summarized in ref. [120]. Indeed, the first data from central Pb–Pb collisions at SPS energy showed a substantial suppression, which could be interpreted in terms of nuclear effects and the Debye screening mechanism. However, the data at RHIC energy exhibited a nearly identical suppression and an unexpected peaking at mid-rapidity[120], which could not be reconciled with the predictions using the colour-screening model. Both observations on the energy and rapidity dependence of R_{AA} for J/ψ mesons were, however, consistent with their thermal origin[107,121], albeit with the qualification of a rather poorly known charm production cross-section.

In the statistical hadronization scenario, the J/ψ nuclear modification factor R_{AA} (see above) is obtained by computing the yields in AA collisions while the yields in proton–proton collisions are taken from experimental data. The R_{AA} value determined in this way should increase with increasing collision energy, implying reduced suppression or even enhancement due to the rapid increase with energy of the charm production cross-section. Clear evidence for such a pattern was obtained with the first ALICE measurements at LHC energy[122]. Since then, a large number of additional data including detailed energy, rapidity, centrality and transverse momentum dependences of R_{AA} for J/ψ as well as hydrodynamic flow and $\psi(2S)/(J/\psi)$ ratio results have provided a firm basis for the statistical hadronization scenario[101], with the biggest uncertainties still related to the not-yet-measured value of the open charm cross-section in central Pb–Pb collisions. Current results for J/ψ yields and interpretation within the statistical hadronization picture are summarized in Fig. 7. A large increase of R_{AA} with increasing collision energy is clearly observed. Furthermore, more recent measurements demonstrate (see, for example, figure 16 in ref. [123]) that the increase is largely concentrated at J/ψ transverse momentum values less than the mass $m_{J/\psi} = 3.1$ GeV. This latter observation was first predicted in ref. [124]. Both provide further support of the original predictions from the statistical hadronization approach.

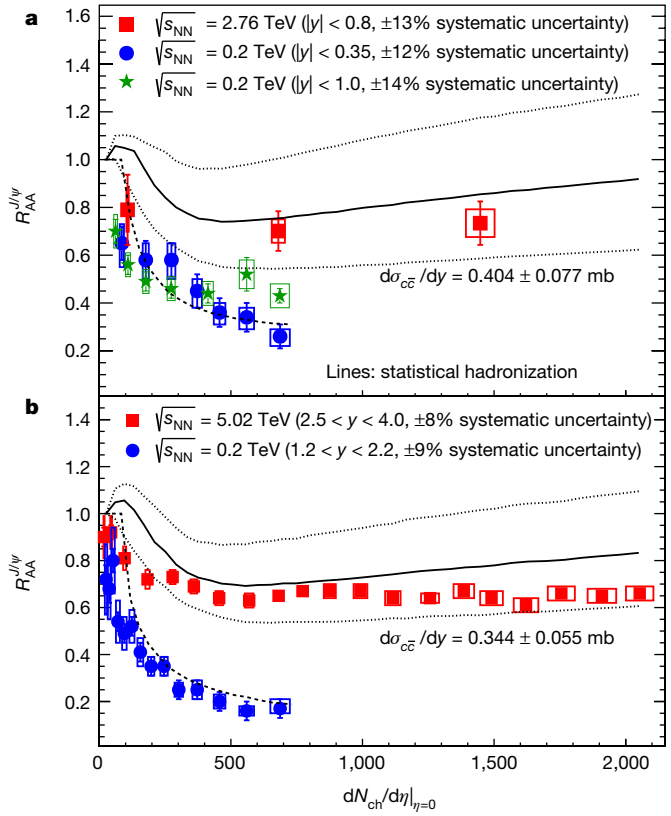

Fig. 7 | The nuclear modification factor R_{AA} for inclusive J/ψ production. a, **b**, The dependence of R_{AA} on the multiplicity density of charged particles N_{ch} per unit of pseudorapidity η, $dN_{ch}/d\eta|_{\eta=0}$ is shown for mid-rapidity (**a**) and forward rapidity (**b**). The data are for Au–Au collisions from the PHENIX Collaboration (blue)[140,141] and the STAR Collaboration (green)[142] at RHIC and for Pb–Pb collisions from the ALICE Collaboration (red)[122,123] at the LHC. The open boxes and error bars show the total systematic and statistical uncertainties, respectively.

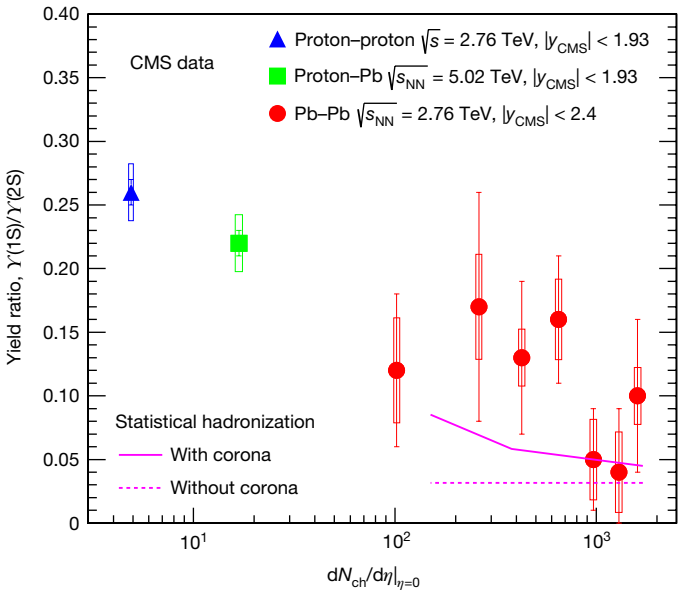

Fig. 8 | Multiplicity dependence of production ratio of bottomonium states $\Upsilon(2S)$ and $\Upsilon(1S)$. The data were measured by the Compact Muon Solenoid (CMS) experiment at the LHC in proton–proton (blue), proton–Pb (green) and Pb–Pb (red) collisions[125]. The magenta lines are statistical hadronization predictions for Pb–Pb collisions; the solid line includes an estimate of the contribution of the production in the corona[101] of the colliding nuclei. The open boxes and error bars show the total systematic and statistical uncertainties, respectively.

Recent measurements of the production of bottomonium states at the LHC[125–127] and at RHIC[128] can provide further insight into the understanding of the production dynamics of quarkonia in nuclear collisions. The nuclear modification factor for the Υ states exhibits, at LHC energies, a suppression pattern[126] not unlike that expected in the original Debye screening scenario[112]. On the other hand, the observed production ratio $\Upsilon(2S)/\Upsilon(1S)$, shown in Fig. 8, is also consistent with a thermalization pattern as one approaches central collisions. Indeed, for central Pb–Pb collisions, this ratio is compatible with the value predicted by the statistical hadronization model for $T \approx 156$ MeV. This provides the tantalizing possibility of adding the bottom flavour as an experimental observable to further constrain the QCD phase boundary with nucleus–nucleus collision data at high energies.

An essential ingredient of the statistical hadronization scenario for heavy quarks is that they can travel, in the QGP, relatively large distances to combine with other uncorrelated partons. The observed increase of the R_{AA} for J/ψ with increasing collision energy strongly supports the notion that the mobility of the heavy quarks is such that it allows travel distances exceeding that of the typical 1-fm hadronic confinement scale. In fact, for LHC energy, the volume of a slice of one unit of rapidity of the fireball exceeds 5,000 fm^3, as shown in section 'Statistical hadronization of light quarks', which implies that charm quarks can travel distances of the order of 10 fm. This results in the possibility of bound-state formation with all other appropriate partons in the medium having statistical weights quantified by the characteristics of the hadron (mass, quantum numbers) at the phase boundary. The results of the charmonium measurements thereby imply a direct connection to the deconfinement properties of the strongly interacting medium created in ultra-relativistic nuclear collisions.

Outlook

The phenomenological observation of the thermal nature of particle production in heavy-ion collisions at the QCD phase boundary in accord with lattice QCD raises a number of challenging theoretical and experimental issues. An intriguing question is how an isolated quantum system such as a fireball formed in relativistic nuclear collisions can reach an apparently equilibrated state. Similar questions appear[129,130] in studies of ultracold quantum gases or black holes and may point to a common solution. A second area of interest is the mechanism for the formation of loosely bound nuclear states in a hot fireball at a temperature exceeding their binding energies by orders of magnitude. The question of whether there exist colourless bound states inside a deconfined QGP is related to the experimentally challenging measurements of excited-state populations of quarkonia.

Another priority for the field is the direct observation of the restoration of chiral symmetry and the related critical behaviour in relativistic nuclear collisions with precision measurements and analysis of fluctuation observables. A highlight would be the observation of a critical endpoint in the QCD phase diagram. Making progress with these fundamental issues is at the heart of many ongoing and future theoretical and experimental investigations.

Note added in proof: The proton anomaly discussed in this Review has recently been explained in terms of a pion–nucleon phase-shift analysis[143]. The precision of the cross-over temperature in LQCD has recently been improved to 156.5 ± 1.5 MeV, in very close agreement with the results obtained here[144].

Received: 6 October 2017; Accepted: 3 July 2018;
Published online 19 September 2018.

1. Gyulassy, M. & McLerran, L. New forms of QCD matter discovered at RHIC. *Nucl. Phys. A* **750**, 30–63 (2005).
2. Braun-Munzinger, P. & Stachel, J. The quest for the quark–gluon plasma. *Nature* **448**, 302–309 (2007).
Concise review of pre-LHC situation and summary of expectations.
3. Jacak, B. V. & Müller, B. The exploration of hot nuclear matter. *Science* **337**, 310–314 (2012).
4. Itoh, N. Hydrostatic equilibrium of hypothetical quark stars. *Prog. Theor. Phys.* **44**, 291–292 (1970).

5. Collins, J. C. & Perry, M. Superdense matter: neutrons or asymptotically free quarks? *Phys. Rev. Lett.* **34**, 1353–1356 (1975).
6. Cabibbo, N. & Parisi, G. Exponential hadronic spectrum and quark liberation. *Phys. Lett. B* **59**, 67–69 (1975).
7. Chapline, G. & Nauenberg, M. Asymptotic freedom and the baryon-quark phase transition. *Phys. Rev. D* **16**, 450–456 (1977).
8. Shuryak, E. V. Quark-gluon plasma and hadronic production of leptons, photons and psions. *Phys. Lett. B* **78**, 150–153 (1978).
9. Boyanovsky, D., de Vega, H. & Schwarz, D. Phase transitions in the early and the present universe. *Annu. Rev. Nucl. Part. Sci.* **56**, 441–500 (2006).
10. Rajagopal, K. & Wilczek, F. in *At The Frontier Of Particle Physics. Handbook of QCD* Vol. 3 (ed. Shifman, M.) 2061–2151 (World Scientific, New Jersey, 2001).
11. Heinz, U. W. & Jacob, M. Evidence for a new state of matter: an assessment of the results from the CERN lead beam program. Preprint at https://arxiv.org/abs/nucl-th/0002042 (2000).
12. E877 Collaboration. Observation of anisotropic event shapes and transverse flow in Au + Au collisions at AGS energy. *Phys. Rev. Lett.* **73**, 2532–2535 (1994).
13. STAR Collaboration. Experimental and theoretical challenges in the search for the quark gluon plasma: the STAR Collaboration's critical assessment of the evidence from RHIC collisions. *Nucl. Phys. A* **757**, 102–183 (2005).
14. BRAHMS Collaboration. Quark gluon plasma and color glass condensate at RHIC? The perspective from the BRAHMS experiment. *Nucl. Phys. A* **757**, 1–27 (2005).
15. PHENIX Collaboration. Formation of dense partonic matter in relativistic nucleus-nucleus collisions at RHIC: experimental evaluation by the PHENIX Collaboration. *Nucl. Phys. A* **757**, 184–283 (2005).
16. PHOBOS Collaboration. The PHOBOS perspective on discoveries at RHIC. *Nucl. Phys. A* **757**, 28–101 (2005).
17. Müller, B., Schukraft, J. & Wyslouch, B. First results from Pb+Pb collisions at the LHC. *Annu. Rev. Nucl. Part. Sci.* **62**, 361–386 (2012).
Impact of the first LHC data on QGP research.
18. Schukraft, J. Heavy ion physics at the Large Hadron Collider: what is new? What is next? *Phys. Scr. T* **158**, 014003 (2013).
19. Braun-Munzinger, P., Koch, V., Schäfer, T. & Stachel, J. Properties of hot and dense matter from relativistic heavy ion collisions. *Phys. Rep.* **621**, 76–126 (2016).
20. Braun-Munzinger, P. & Wambach, J. The phase diagram of strongly-interacting matter. *Rev. Mod. Phys.* **81**, 1031–1050 (2009).
21. Müller, B. Investigation of hot QCD matter: theoretical aspects. *Phys. Scr. T* **158**, 014004 (2013).
22. Satz, H. Probing the states of matter in QCD. *Int. J. Mod. Phys. A* **28**, 1330043 (2013).
23. Particle Data Group Collaboration. Review of particle physics. *Chin. Phys. C* **40**, 100001 (2016).
24. Gross, D. J. & Wilczek, F. Ultraviolet behavior of nonabelian gauge theories. *Phys. Rev. Lett.* **30**, 1343–1346 (1973).
25. Politzer, H. D. Reliable perturbative results for strong interactions? *Phys. Rev. Lett.* **30**, 1346–1349 (1973).
26. Karsch, F. Lattice QCD at high temperature and density. *Lect. Notes Phys.* **583**, 209–249 (2002).
27. Wilczek, F. QCD made simple. *Phys. Today* **53**, 22–28 (2000).
28. Bazavov, A. et al. The chiral and deconfinement aspects of the QCD transition. *Phys. Rev. D* **85**, 054503 (2012).
29. Aoki, Y., Endrodi, G., Fodor, Z., Katz, S. & Szabo, K. The order of the quantum chromodynamics transition predicted by the standard model of particle physics. *Nature* **443**, 675–678 (2006).
30. HotQCD Collaboration. The equation of state in (2+1)-flavor QCD. *Phys. Rev. D* **90**, 094503 (2014).
Determination of the equation of state of hot QGP from LQCD.
31. Borsányi, S. et al. Is there still any T_c mystery in lattice QCD? Results with physical masses in the continuum limit III. *J. High Energy Phys.* **9**, 73 (2010).
32. Borsányi, S. et al. Full result for the QCD equation of state with 2+1 flavors. *Phys. Lett. B* **730**, 99–104 (2014).
33. Luo, X. & Xu, N. Search for the QCD critical point with fluctuations of conserved quantities in relativistic heavy-ion collisions at RHIC: an overview. *Nucl. Sci. Tech.* **28**, 112 (2017).
34. Karsch, F. The last word(s) on CPOD 2013. *Proc. Sci.* **185**, 46 (2013).
35. Dürr, S. et al. Ab-initio determination of light hadron masses. *Science* **322**, 1224–1227 (2008).
36. Bazavov, A. et al. The QCD equation of state to $\mathcal{O}\left(\mu_B^6\right)$ from lattice QCD. *Phys. Rev. D* **95**, 054504 (2017).
37. Andronic, A., Braun-Munzinger, P., Stachel, J. & Winn, M. Interacting hadron resonance gas meets lattice QCD. *Phys. Lett. B* **718**, 80–85 (2012).
38. Karsch, F. Thermodynamics of strong interaction matter from lattice QCD and the hadron resonance gas model. *Acta Phys. Polon. B* **7**, 117–126 (2014).
39. Dashen, R., Ma, S.-K. & Bernstein, H. J. S Matrix formulation of statistical mechanics. *Phys. Rev.* **187**, 345–370 (1969).
40. Cleymans, J. & Satz, H. Thermal hadron production in high-energy heavy ion collisions. *Z. Phys. C* **57**, 135–147 (1993).
41. Braun-Munzinger, P., Stachel, J., Wessels, J. & Xu, N. Thermal equilibration and expansion in nucleus-nucleus collisions at the AGS. *Phys. Lett. B* **344**, 43–48 (1995).
Comprehensive application of the statistical hadronization model to data.
42. Braun-Munzinger, P., Redlich, K. & Stachel, J. in *Quark Gluon Plasma* Vol. 3 (eds Hwa, R. C. & Wang, X.-N.) 491–599 (World Scientific, Singapore, 2004).
43. Braun-Munzinger, P., Magestro, D., Redlich, K. & Stachel, J. Hadron production in Au–Au collisions at RHIC. *Phys. Lett. B* **518**, 41–46 (2001).
Establishing the statistical hadronization model in the RHIC era.
44. Letessier, J. & Rafelski, J. Hadron production and phase changes in relativistic heavy ion collisions. *Eur. Phys. J. A* **35**, 221–242 (2008).
45. Stachel, J., Andronic, A., Braun-Munzinger, P. & Redlich, K. Confronting LHC data with the statistical hadronization model. *J. Phys. Conf. Ser.* **509**, 012019 (2014).
46. Hagedorn, R. How we got to QCD matter from the hadron side by trial and error. *Lect. Notes Phys.* **221**, 53–76 (1985).
47. Cleymans, J. & Redlich, K. Unified description of freezeout parameters in relativistic heavy ion collisions. *Phys. Rev. Lett.* **81**, 5284–5286 (1998).
First interpretation of the chemical freeze-out line.
48. Stock, R. The parton to hadron phase transition observed in Pb+Pb collisions at 158-GeV per nucleon. *Phys. Lett. B* **456**, 277–282 (1999).
49. Braun-Munzinger, P. & Stachel, J. Particle ratios, equilibration, and the QCD phase boundary. *J. Phys. G* **28**, 1971–1976 (2002).
50. Braun-Munzinger, P., Stachel, J. & Wetterich, C. Chemical freezeout and the QCD phase transition temperature. *Phys. Lett. B* **596**, 61–69 (2004).
51. Andronic, A., Braun-Munzinger, P. & Stachel, J. Thermal hadron production in relativistic nuclear collisions: the hadron mass spectrum, the horn, and the QCD phase transition. *Phys. Lett. B* **673**, 142–145 (2009).
52. Floerchinger, S. & Wetterich, C. Chemical freeze-out in heavy ion collisions at large baryon densities. *Nucl. Phys. A* **890–891**, 11–24 (2012).
53. Bazavov, A. et al. Freeze-out conditions in heavy ion collisions from QCD thermodynamics. *Phys. Rev. Lett.* **109**, 192302 (2012).
54. ALICE Collaboration. Centrality dependence of π, K, p production in Pb-Pb collisions at $\sqrt{s_{\rm NN}} = 2.76$ TeV. *Phys. Rev. C* **88**, 044910 (2013).
55. ALICE Collaboration. K^0_S and Λ production in Pb-Pb collisions at $\sqrt{s_{\rm NN}} = 2.76$ TeV. *Phys. Rev. Lett.* **111**, 222301 (2013).
56. ALICE Collaboration. Multi-strange baryon production at mid-rapidity in Pb-Pb collisions at $\sqrt{s_{\rm NN}} = 2.76$ TeV. *Phys. Lett. B* **728**, 216–227 (2014).
57. ALICE Collaboration. $K^*(892)^0$ and $\phi(1020)$ production in Pb-Pb collisions at $\sqrt{s_{\rm NN}} = 2.76$ TeV. *Phys. Rev. C* **91**, 024609 (2015).
58. ALICE Collaboration. $^3_1$H and $^3_{\bar{1}}\overline{\rm H}$ production in Pb-Pb collisions at $\sqrt{s_{\rm NN}} = 2.76$ TeV. *Phys. Lett. B* **754**, 360–372 (2016).
59. ALICE Collaboration. Production of light nuclei and anti-nuclei in *pp* and Pb-Pb collisions at energies available at the CERN Large Hadron Collider. *Phys. Rev. C* **93**, 024917 (2016).
60. ALICE Collaboration. Production of ^{4}He and $\overline{^4\rm He}$ in Pb–Pb collisions at $\sqrt{s_{\rm NN}} =$ 2.76 TeV at the LHC. *Nucl. Phys. A* **971**, 1–20 (2018).
61. ALICE Collaboration. Pion, kaon, and proton production in central Pb–Pb collisions at $\sqrt{s_{\rm NN}} = 2.76$ TeV. *Phys. Rev. Lett.* **109**, 252301 (2012).
62. Becattini, F., Grossi, E., Bleicher, M., Steinheimer, J. & Stock, R. Centrality dependence of hadronization and chemical freeze-out conditions in heavy ion collisions at $\sqrt{s_{\rm NN}} = 2.76$ TeV. *Phys. Rev. C* **90**, 054907 (2014).
63. ALICE Collaboration. Enhanced production of multi-strange hadrons in high-multiplicity proton-proton collisions. *Nat. Phys.* **13**, 535–539 (2017).
64. Andronic, A., Braun-Munzinger, P., Stachel, J. & Stöcker, H. Production of light nuclei, hypernuclei and their antiparticles in relativistic nuclear collisions. *Phys. Lett. B* **697**, 203–207 (2011).
65. Chapline, G. & Kerman, A. *On the Possibility of Making Quark Matter in Nuclear Collisions*. Report No. MIT-CTP-695, https://inspirehep.net/record/134446/files/CTP-695.pdf (MIT Center of Theoretical Physics, 1978).
66. Csernai, L. P. & Kapusta, J. I. Entropy and cluster production in nuclear collisions. *Phys. Rep.* **131**, 223–318 (1986).
67. Hirenzaki, S., Suzuki, T. & Tanihata, I. A general formula of the coalescence model. *Phys. Rev. C* **48**, 2403–2408 (1993).
68. ExHIC Collaboration. Exotic hadrons from heavy ion collisions. *Prog. Part. Nucl. Phys.* **95**, 279–322 (2017).
69. NPLQCD Collaboration. Light nuclei and hypernuclei from quantum chromodynamics in the limit of SU(3) flavor symmetry. *Phys. Rev. D* **87**, 034506 (2013).
70. Hagedorn, R. & Redlich, K. Statistical thermodynamics in relativistic particle and ion physics: canonical or grand canonical? *Z. Phys. C* **27**, 541–551 (1985).
Theoretical foundations of the statistical thermodynamics of particle production.
71. Hamieh, S., Redlich, K. & Tounsi, A. Canonical description of strangeness enhancement from p–A to Pb–Pb collisions. *Phys. Lett. B* **486**, 61–66 (2000).
72. Braun-Munzinger, P. & Stachel, J. (Non)thermal aspects of charmonium production and a new look at J/ψ suppression. *Phys. Lett. B* **490**, 196–202 (2000).
Statistical hadronization model for heavy quarks.
73. NA57 Collaboration. Energy dependence of hyperon production in nucleus nucleus collisions at SPS. *Phys. Lett. B* **595**, 68–74 (2004).
74. Becattini, F. A thermodynamical approach to hadron production in e^+e^- collisions. *Z. Phys. C* **69**, 485–492 (1996).
75. Becattini, F., Castorina, P., Manninen, J. & Satz, H. The thermal production of strange and non-strange hadrons in e^+e^- collisions. *Eur. Phys. J. C* **56**, 493–510 (2008).
76. Andronic, A., Beutler, F., Braun-Munzinger, P., Redlich, K. & Stachel, J. Thermal description of hadron production in e^+e^- collisions revisited. *Phys. Lett. B* **675**, 312–318 (2009).
77. STAR Collaboration. Bulk properties of the medium produced in relativistic heavy-ion collisions from the beam energy scan program. *Phys. Rev. C* **96**, 044904 (2017).
78. Cleymans, J., Oeschler, H. & Redlich, K. Influence of impact parameter on thermal description of relativistic heavy ion collisions at (1–2)*A* GeV. *Phys. Rev. C* **59**, 1663–1673 (1999).

79. Braun-Munzinger, P., Heppe, I. & Stachel, J. Chemical equilibration in Pb + Pb collisions at the SPS. *Phys. Lett. B* **465**, 15–20 (1999).
80. Manninen, J. & Becattini, F. Chemical freeze-out in ultra-relativistic heavy ion collisions at $\sqrt{s_{NN}}$ = 130 and 200 GeV. *Phys. Rev. C* **78**, 054901 (2008).
81. STAR Collaboration. Identified particle production, azimuthal anisotropy, and interferometry measurements in Au+Au collisions at $\sqrt{s_{NN}}$ = 9.2 GeV. *Phys. Rev. C* **81**, 024911 (2010).
82. Braun-Munzinger, P. & Stachel, J. Dynamics of ultrarelativistic nuclear collisions with heavy beams: an experimental overview. *Nucl. Phys. A* **638**, 3c–18c (1998).
Establishing the boundary line for chemical freeze-out.
83. Hagedorn, R. Statistical thermodynamics of strong interactions at high-energies. *Nuovo Cim.* **3** (Suppl.), 147–186 (1965).
84. Hagedorn, R. *Miscellaneous Elementary Remarks about the Phase Transition from a Hadron Gas to a Quark-Gluon Plasma*. Report No. CERN-TH-4100, http://cds.cern.ch/record/158166/files/198504017.pdf (CERN, 1985).
85. Stephanov, M. A., Rajagopal, K. & Shuryak, E. V. Signatures of the tricritical point in QCD. *Phys. Rev. Lett.* **81**, 4816–4819 (1998).
86. Braun-Munzinger, P., Cleymans, J., Oeschler, H. & Redlich, K. Maximum relative strangeness content in heavy ion collisions around 30 GeV/A. *Nucl. Phys. A* **697**, 902–912 (2002).
87. ALICE Collaboration. Centrality dependence of the charged-particle multiplicity density at midrapidity in Pb-Pb collisions at $\sqrt{s_{NN}}$ = 5.02 TeV. *Phys. Rev. Lett.* **116**, 222302 (2016).
88. Dainese, A. et al. Heavy ions at the Future Circular Collider. *CERN Yellow Rep.* **3**, 635–691 (2017); https://e-publishing.cern.ch/index.php/CYRM/article/view/515/371.
89. Pierre Auger Collaboration. Ultra-high energy cosmic rays: recent results and future plans of Auger. *AIP Conf. Proc.* **1852**, 040001 (2017).
90. Borsanyi, S. et al. QCD equation of state at nonzero chemical potential: continuum results with physical quark masses at order μ^2. *J. High Energy Phys.* **8**, 53 (2012).
91. PHENIX Collaboration. Enhanced production of direct photons in Au+Au collisions at $\sqrt{s_{NN}}$ = 200 GeV and implications for the initial temperature. *Phys. Rev. Lett.* **104**, 132301 (2010).
92. ALICE Collaboration. Direct photon production in Pb-Pb collisions at $\sqrt{s_{NN}}$ = 2.76 TeV. *Phys. Lett. B* **754**, 235–248 (2016).
93. Braun-Munzinger, P., Kalweit, A., Redlich, K. & Stachel, J. Confronting fluctuations of conserved charges in central nuclear collisions at the LHC with predictions from lattice QCD. *Phys. Lett. B* **747**, 292–298 (2015).
94. Karsch, F. Determination of freeze-out conditions from lattice QCD calculations. *Cent. Eur. J. Phys.* **10**, 1234–1237 (2012).
95. Borsanyi, S. et al. Freeze-out parameters from electric charge and baryon number fluctuations: is there consistency? *Phys. Rev. Lett.* **113**, 052301 (2014).
96. PHENIX Collaboration. Measurement of higher cumulants of net-charge multiplicity distributions in Au+Au collisions at $\sqrt{s_{NN}}$ = 7.7–200 GeV. *Phys. Rev. C* **93**, 011901 (2016).
97. Braun-Munzinger, P. & Redlich, K. Charmonium production from the secondary collisions at LHC energy. *Eur. Phys. J. C* **16**, 519–525 (2000).
98. Zhang, B.-W., Ko, C.-M. & Liu, W. Thermal charm production in a quark-gluon plasma in Pb-Pb collisions at $\sqrt{s_{NN}}$ = 25.5 TeV. *Phys. Rev. C* **77**, 024901 (2008).
99. Zhou, K., Chen, Z., Greiner, C. & Zhuang, P. Thermal charm and charmonium production in quark gluon plasma. *Phys. Lett. B* **758**, 434–439 (2016).
100. Cacciari, M. et al. Theoretical predictions for charm and bottom production at the LHC. *J. High Energy Phys.* **10**, 137 (2012).
101. Andronic, A., Braun-Munzinger, P., Redlich, K. & Stachel, J. Statistical hadronization of heavy quarks in ultra-relativistic nucleus-nucleus collisions. *Nucl. Phys. A* **789**, 334–356 (2007). **Working out predictions for charmonium and bottomonium production at collider energies.**
102. ALICE Collaboration. Suppression of high transverse momentum D mesons in central Pb-Pb collisions at $\sqrt{s_{NN}}$ = 2.76 TeV. *J. High Energy Phys.* **9**, 112 (2012).
103. ALICE Collaboration. *D* meson elliptic flow in noncentral Pb-Pb collisions at $\sqrt{s_{NN}}$ = 2.76 TeV. *Phys. Rev. Lett.* **111**, 102301 (2013).
104. STAR Collaboration. Observation of D^0 meson nuclear modifications in Au+Au collisions at $\sqrt{s_{NN}}$ = 200 GeV. *Phys. Rev. Lett.* **113**, 142301 (2014).
105. Matsui, T. & Satz, H. J/ψ suppression by quark-gluon plasma formation. *Phys. Lett. B* **178**, 416–422 (1986).
Debye screening of J/ψ mesons in a QGP.
106. Vogt, R. J/ψ production and suppression. *Phys. Rep.* **310**, 197–260 (1999).
107. Braun-Munzinger, P. & Stachel, J. in *Relativistic Heavy Ion Physics* (ed. Stock, R.) 424–444 (*Landolt-Börnstein – Group I: Elementary Particles, Nuclei and Atoms* Vol. 23, Springer, Berlin, 2010).
108. Andronic, A., Braun-Munzinger, P., Redlich, K. & Stachel, J. The thermal model on the verge of the ultimate test: particle production in Pb-Pb collisions at the LHC. *J. Phys. G* **38**, 124081 (2011).
109. Thews, R. L., Schroedter, M. & Rafelski, J. Enhanced J/ψ production in deconfined quark matter. *Phys. Rev. C* **63**, 054905 (2001).
Continuous formation and destruction of charmonia in the QGP.
110. Liu, Y.-P., Qu, Z., Xu, N. & Zhuang, P.-F. J/ψ transverse momentum distribution in high energy nuclear collisions at RHIC. *Phys. Lett. B* **678**, 72–76 (2009).
111. Grandchamp, L., Rapp, R. & Brown, G. E. In medium effects on charmonium production in heavy ion collisions. *Phys. Rev. Lett.* **92**, 212301 (2004).
112. Emerick, A., Zhao, X. & Rapp, R. Bottomonia in the quark-gluon plasma and their production at RHIC and LHC. *Eur. Phys. J. A* **48**, 72 (2012).
113. Zhou, K., Xu, N., Xu, Z. & Zhuang, P. Medium effects on charmonium production at ultrarelativistic energies available at the CERN Large Hadron Collider. *Phys. Rev. C* **89**, 054911 (2014).
114. NA50 Collaboration. ψ' production in Pb-Pb collisions at 158 GeV/nucleon. *Eur. Phys. J. C* **49**, 559–567 (2007).
115. ALICE Collaboration. J/ψ elliptic flow in Pb–Pb collisions at $\sqrt{s_{NN}}$ =2.76 TeV. *Phys. Rev. Lett.* **111**, 162301 (2013).
116. ALICE Collaboration. J/ψ elliptic flow in Pb-Pb collisions at $\sqrt{s_{NN}}$ = 5.02 TeV. *Phys. Rev. Lett.* **119**, 242301 (2017).
117. ALICE Collaboration. D-meson azimuthal anisotropy in mid-central Pb-Pb collisions at $\sqrt{s_{NN}}$ = 5.02 TeV. *Phys. Rev. Lett.* **120**, 102301 (2018).
118. STAR Collaboration. Measurement of J/ψ azimuthal anisotropy in Au+Au collisions at $\sqrt{s_{NN}}$ = 200 GeV. *Phys. Rev. Lett.* **111**, 052301 (2013).
119. NA50 Collaboration. J/ψ azimuthal anisotropy relative to the reaction plane in Pb-Pb collisions at 158 GeV per nucleon. *Eur. Phys. J. C* **61**, 853–858 (2009).
120. Kluberg, L. & Satz, H. in *Relativistic Heavy Ion Physics* (ed. Stock, R.) 373–423 (*Landolt-Börnstein – Group I: Elementary Particles, Nuclei and Atoms* Vol. 23, Springer, Berlin, 2010).
121. Andronic, A., Braun-Munzinger, P., Redlich, K. & Stachel, J. Evidence for charmonium generation at the phase boundary in ultra-relativistic nuclear collisions. *Phys. Lett. B* **652**, 259–261 (2007).
122. ALICE Collaboration. Centrality, rapidity and transverse momentum dependence of J/ψ suppression in Pb-Pb collisions at $\sqrt{s_{NN}}$ = 2.76 TeV. *Phys. Lett. B* **743**, 314–327 (2014).
First experimental evidence of reduced J/ψ suppression at LHC energy.
123. ALICE Collaboration. J/ψ suppression at forward rapidity in Pb-Pb collisions at $\sqrt{s_{NN}}$ = 5.02 TeV. *Phys. Lett. B* **766**, 212–224 (2017).
124. Zhao, X. & Rapp, R. Medium modifications and production of charmonia at LHC. *Nucl. Phys. A* **859**, 114–125 (2011).
125. CMS Collaboration. Event activity dependence of $\Upsilon(nS)$ production in $\sqrt{s_{NN}}$=5.02 TeV pPb and $\sqrt{s_{NN}}$=2.76 TeV pp collisions. *J. High Energy Phys.* **4**, 103 (2014).
126. CMS Collaboration. Observation of sequential Υ suppression in PbPb collisions. *Phys. Rev. Lett.* **109**, 222301 (2012).
127. ALICE Collaboration. Suppression of $\Upsilon(1S)$ at forward rapidity in Pb–Pb collisions at $\sqrt{s_{NN}}$ = 2.76 TeV. *Phys. Lett. B* **738**, 361–372 (2014).
128. PHENIX Collaboration. Measurement of $\Upsilon(1S + 2S + 3S)$ production in p+p and Au+Au collisions at $\sqrt{s_{NN}}$ = 200 GeV. *Phys. Rev. C* **91**, 024913 (2015).
129. Rigol, M., Dunjko, V. & Olshanii, M. Thermalization and its mechanism for generic isolated quantum systems. *Nature* **452**, 854–858 (2008).
130. Gring, M. et al. Relaxation and prethermalization in an isolated quantum system. *Science* **337**, 1318–1322 (2012).
131. Andronic, A. An overview of the experimental study of quark-gluon matter in high-energy nucleus-nucleus collisions. *Int. J. Mod. Phys. A* **29**, 1430047 (2014).
132. Vovchenko, V., Begun, V. V. & Gorenstein, M. I. Hadron multiplicities and chemical freeze-out conditions in proton-proton and nucleus-nucleus collisions. *Phys. Rev. C* **93**, 064906 (2016).
133. Becattini, F., Steinheimer, J., Stock, R. & Bleicher, M. Hadronization conditions in relativistic nuclear collisions and the QCD pseudo-critical line. *Phys. Lett. B* **764**, 241–246 (2017).
134. NA51 Collaboration. J/ψ, ψ' and Drell-Yan production in pp and pd interactions at 450 GeV/c. *Phys. Lett. B* **438**, 35–40 (1998).
135. HERA-B Collaboration. A measurement of the ψ' to J/ψ production ratio in 920-GeV proton-nucleus interactions. *Eur. Phys. J. C* **49**, 545–558 (2007).
136. PHENIX Collaboration. Measurement of the relative yields of $\psi(2S)$ to $\psi(1S)$ mesons produced at forward and backward rapidity in p+p, p+Al, p+Au and 3He+Au collisions at $\sqrt{s_{NN}}$ = 200 GeV. *Phys. Rev. C* **95**, 034904 (2017).
137. LHCb Collaboration. Measurement of J/ψ production in pp collisions at $\sqrt{s}$ = 7 TeV. *Eur. Phys. J. C* **71**, 1645 (2011).
138. LHCb Collaboration. Measurement of $\psi(2S)$ meson production in pp collisions at $\sqrt{s}$ =7 TeV. *Eur. Phys. J. C* **72**, 2100 (2012).
139. ALICE Collaboration. Energy dependence of forward-rapidity J/ψ and $\psi(2S)$ production in pp collisions at the LHC. *Eur. Phys. J. C* **77**, 392 (2017).
140. PHENIX Collaboration. J/ψ production vs centrality, transverse momentum, and rapidity in Au+Au collisions at $\sqrt{s_{NN}}$ = 200 GeV. *Phys. Rev. Lett.* **98**, 232301 (2007).
141. PHENIX Collaboration. J/ψ suppression at forward rapidity in Au+Au collisions at $\sqrt{s_{NN}}$ = 200 GeV. *Phys. Rev. C* **84**, 054912 (2011).
142. STAR Collaboration. J/ψ production at low p_T in Au+Au and Cu+Cu collisions at $\sqrt{s_{NN}}$ = 200 GeV at STAR. *Phys. Rev. C* **90**, 024906 (2014).
143. Andronic, A. et al. The thermal proton yield anomaly in Pb-Pb collisions at the LHC and its resolution. Preprint at https://arxiv.org/abs/1808.03102 (2018).
144. Steinbrecher, P. The QCD crossover at zero and non-zero baryon densities from lattice QCD. Preprint at https://arxiv.org/abs/1807.05607 (2018).

Acknowledgements K.R. acknowledges support by the Polish National Science Centre under Maestro grant DEC-2013/10/A/ST2/00106. This work is part of and supported by the DFG Collaborative Research Centre 'SFB1225/ISOQUANT'.

Author contributions All authors contributed equally to the physics analysis and to writing the manuscript.

Competing interests The authors declare no competing interests.

Additional information
Reprints and permissions information is available at http://www.nature.com/reprints.
Correspondence and requests for materials should be addressed to P.B.-M.
Publisher's note: Springer Nature remains neutral with regard to jurisdictional claims in published maps and institutional affiliations.